Effect of Si doping on electrical and optical properties of ZnO thin films grown by sequential pulsed laser deposition

2009 J. Phys. D: Appl. Phys. 42 165405

(http://iopscience.iop.org/0022-3727/42/16/165405)

J. Phys. D: Appl. Phys. **42** (2009) 165405 (7pp) doi:10.1088/0022-3727/42/16/165405

Effect of Si doping on electrical and optical properties of ZnO thin films grown by sequential pulsed laser deposition

A K Das[1], **P Misra and L M Kukreja**

Laser Materials Processing Division, Raja Ramanna Centre for Advanced Technology, Indore 452 013, India

E-mail: amitdas@rrcat.gov.in

Received 31 March 2009, in final form 30 June 2009
Published 31 July 2009
Online at stacks.iop.org/JPhysD/42/165405

Abstract

The sequential pulsed laser deposition technique was used to grow highly transparent and *c*-axis oriented thin films of Si doped ZnO on sapphire substrates. On doping with Si, the resistivity of the virgin ZnO thin films was found to decrease from $\sim 3.0 \times 10^{-2}$ to $6.2 \times 10^{-4}\,\Omega\,\mathrm{cm}$ and its bandgap increased from about 3.28 to 3.44 eV at different doping concentrations. XPES measurements revealed that Si predominantly occupies the Zn lattice sites in the Si^{+3} state. The increase in the bandgap of the ZnO films with increasing Si concentration was found to be due to the collective effects of high carrier concentration induced Burstein–Moss blue shift and bandgap narrowing. Efficient photoluminescence (PL) was observed at room temperature from these Si doped ZnO films. The bandgaps obtained from the PL measurements were found to be Stokes shifted as compared with those obtained from the transmission spectra. Si doping of ZnO offers the possibility of developing superior transparent conducting electrodes for applications such as in display panels, solar cells and transparent resistive non-volatile memories.

1. Introduction

ZnO is a widely known wide and direct bandgap semiconductor with a bandgap of ~3.38 eV at room temperature [1–3]. It crystallizes in the rugged wurtzite structure and is a nominally n-type conductor perhaps due to the presence of native defects such as Zn interstitials, oxygen vacancies [4–7] and/or hydrogen [8]. These two properties, i.e. high transparency in the visible spectral region and good electrical conductivity, make ZnO a suitable material for transparent conducting electrodes (TCE) for display panels, solar cells, transparent non-volatile memories, etc. The resistivity of as-grown ZnO films is generally low $\sim 10^{-1}\,\Omega\,\mathrm{cm}$ [9]. It can be further decreased by suitable donor (group III) dopants such as Al, Ga and In [9–14], which increase the carrier concentration and hence the conductivity of ZnO film. For example, in the case of Ga doped ZnO, the minimum resistivity has been found to be $\sim 8.12 \times 10^{-5}\,\Omega\,\mathrm{cm}$ with a carrier concentration of $\sim 10^{22}\,\mathrm{cm}^{-3}$ [13] at a Ga concentration of ~5 wt%. Others have also found minimum resistivity varying from $\sim 8.1 \times 10^{-5}$–$1.69 \times 10^{-3}\,\Omega\,\mathrm{cm}$ [9, 10, 12] in Ga doped ZnO films. In the case of Al doped ZnO the resistivity was found to be about $1.3 \times 10^{-4}\,\Omega\,\mathrm{cm}$ [14]. Si, being in group IV, may also act as a potential donor and hence enhance the carrier concentration and conductivity of ZnO. In the literature, we could find only one report on Si doping of ZnO by Minami *et al* [15]. They have used RF magnetron sputtering to grow Si doped ZnO thin films and obtained a minimum resistivity of $\sim 3.8 \times 10^{-4}\,\Omega\,\mathrm{cm}$. The bandgap of these films was found to increase with increasing Si concentration in the films; however, no detailed correlation of the observed bandgap variation with Si doping concentration was reported.

We have used sequential pulsed laser deposition to grow highly *c*-axis oriented Si doped ZnO thin films with different Si concentrations on sapphire substrates. The Si concentration in these films was varied by controlling the total ablation time of the Si target compared with that of the ZnO. The sequential ablation technique had earlier been successfully applied for the controlled growth of Sn doped CdO films and ternary alloy $Cd_xZn_{1-x}O$ thin films using two separate targets of SnO_2–CdO and ZnO–CdO, respectively [16, 17]. By using this

[1] Author to whom any correspondence should be addressed.

technique we could successfully deposit Si doped ZnO thin films with different Si concentrations wherein the electrical resistivity of the virgin ZnO films was found to decrease from $\sim 3.0 \times 10^{-2}$ to $\sim 6.2 \times 10^{-4}\,\Omega\,\mathrm{cm}$ with increasing Si ablation duration with respect to that of ZnO. This was accompanied by the increase in its bandgap from ∼3.28 to 3.44 eV. This increase in the ZnO bandgap with increasing Si concentration was explained by considering collectively the Moss–Burstein (BM) shift and bandgap narrowing effects arising due to high carrier and impurity concentration. We have also observed room temperature near band edge photoluminescence (PL) from Si doped ZnO films. The results of these experimental studies are presented and discussed in this paper.

2. Experimental

All the films were grown on single crystal (0 0 0 1) sapphire substrates by sequential ablation of separate ZnO and Si targets using the 3rd harmonic of a Q-switched Nd : YAG laser (355 nm, 10 Hz and 6 ns) at a fluence of $\sim 1\,\mathrm{J\,cm^{-2}}$. The ZnO target was prepared in-house by palletizing the high purity (99.9995%) ZnO powder which was subsequently sintered at 1200 °C for 2 h. The single crystal Si wafer was used as the other target. Concentration of Si in the films was controlled by varying the ablation time of the ZnO target with respect to that of Si, which was kept constant at 1 s using a programmable shutter. The ZnO ablation time was varied in the range 10–50 s in different samples. These sequences were repeated a number of times to get the desired film thicknesses of ∼150 nm in each case, which was measured using a DEKTAK surface profilometer. The sapphire substrates were cleaned prior to deposition using the traditional organic cleaning procedure by boiling them for 5 min each in tricholoro-ethylene, acetone and methanol and then rinsed thoroughly in deionized (DI) water and finally dried using dry nitrogen gas jet. The deposition chamber was initially evacuated to a base pressure of $\sim 1 \times 10^{-6}$ mbar using a turbo-molecular pump and during the deposition a pressure of $\sim 1 \times 10^{-4}$ mbar of flowing high purity oxygen gas (99.999%) was maintained. The substrate temperature was kept at ∼600 °C with an accuracy of ±1 °C to facilitate homogenized doping of Si in ZnO.

The composition of Si doped ZnO thin films was studied using energy dispersive x-ray (EDX) measurements with a Phillips XL 30 CP system. The crystalline characteristics of these films were studied using a high resolution x-ray diffractometer (Philips X'pert MRD) with a resolution of ∼5 arcsec. The optical properties of these films were studied at room temperature using optical transmission and photoluminescence spectroscopy. A UV–visible spectrophotometer (Shimadzu UVPC 3200) was used to record the transmission spectra of these films at room temperature. For PL measurements a 20 mW HeCd laser operating at 325 nm was used as an excitation source and luminescence was collected and detected through a $\frac{1}{2}$ m long spectrometer (Triax 550, Jobin Yvon, France) attached with a CCD detector (Andor, UK). The carrier concentration, mobility and resistivity of these films were measured by using Hall measurement in a four-probe van der Pauw configuration.

Table 1. Dependence of Si concentration on (T_{Si}/T_{ZnO}).

Si to ZnO ablation duration ratio (T_{Si}/T_{ZnO})	Si Concentration as measured from EDX (at%)
0.02	0.5
0.04	1.1
0.07	4.1
0.10	6.5

For these measurements, indium contacts were made on the films which were subsequently annealed in vacuum at ∼400 °C for ∼2 min to allow proper mixing of the indium with that of the ZnO films. The I–V measurements were carried out to ensure the ohmic nature of these contacts.

3. Results and discussion

The incorporation of Si in the ZnO matrix was confirmed by EDX measurement which showed a conspicuous peak of Si besides the characteristic peaks of Zn and O. The concentration of Si in the films was estimated using the respective EDX spectra and is shown in table 1. It can be seen that the Si concentration in these films increased monotonically with increasing Si to ZnO ablation duration ratio (T_{Si}/T_{ZnO}). The incorporation of Si in ZnO along the growth direction can be considered to be uniform due to the fact that the thickness of the grown ZnO layer in each sequence varies from 1 to 5 nm for different samples considering a growth rate of $0.1\,\mathrm{nm\,s^{-1}}$. In a work by Skriniarova *et al* [18], the diffusion lengths of Si in ZnO in the case of ZnO : Al films deposited on the Si substrate by sputtering and subsequently annealed at 500 °C were reported to be about 8 and 14 nm, respectively, for the as-grown and the annealed samples as measured by SIMS. In our case the thickness of the ZnO layer was much less than the reported diffusion lengths of Si in ZnO and the deposition temperature was higher ∼600 °C. Moreover, the kinetic energy of impinging plume particles in the case of PLD is very high compared with that in sputtering. In addition in our films each ZnO layer is sandwiched between two Si layers. So it is expected that Si will diffuse into every ZnO layer both from the top and from the bottom interface resulting nearly uniform distribution of Si in ZnO in the growth direction. The values of lattice spacing (d) and the c-axis lattice parameter as well as the bandgap showed monotonic increase with increasing Si concentration, which is an indication of proper mixing of Si in ZnO along the growth direction. Earlier Misra *et al* [17] had also found using RBS in the case of ZnO–CdO two target ablation that the mixing of ZnO and CdO in the growth direction was uniform.

Figure 1 shows normal θ–2θ x-ray diffraction (XRD) patterns of the Si doped ZnO films with Si concentration of ∼0.5% and that of pure ZnO thin film grown under the same deposition conditions for comparison. The ω rocking curves of the (0 0 0 2) ZnO peak for both the films are shown in the inset of the same figure. It can be seen that the ZnO thin films with and without Si doping are both highly c-axis oriented and

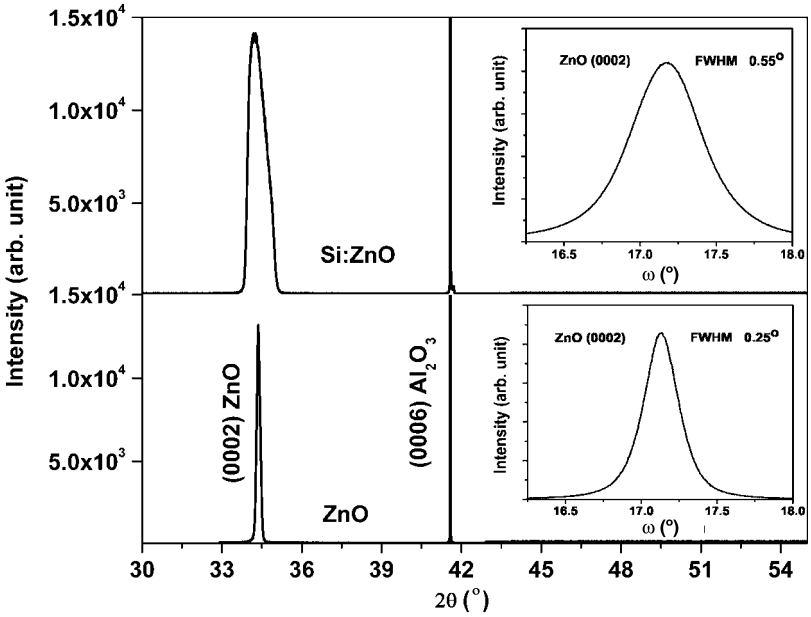

Figure 1. Normal θ–2θ XRD pattern of pure ZnO and ∼0.5 at% Si doped ZnO films. The insets show the corresponding ω rocking curves.

in the pure wurtzite phase having only the (0 0 0 2) reflection of ZnO. The full width at half maximum (FWHM) of the ω rocking curve of the (0 0 0 2) Si : ZnO peak was found to be ∼0.55° compared with ∼0.25° for the undoped ZnO thin films, indicating deterioration in the crystalline quality due to enhancement in the strain and other crystalline defects on doping with Si. However, the resulting broadening of the (0 0 0 2) ZnO peak with increasing Si concentration is found to be within the limits of suitability for its application as TCE. One may notice here that the normal XRD pattern of Si : ZnO appears to be slightly asymmetric and broadened around the central peak. The broadening of the XRD peak in the θ–2θ scan arises either due to limited vertical coherence length or micro-strain. In our case, since the thickness of the film is about 150 nm, it does not contribute significantly to broadening. On the other hand, the micro-strain which is related to the density of point defects and other structural defects arising due to Si doping seems to be mainly responsible for the observed unusual broadening of the peak. Inhomogeneous in-plane distribution of these point defects throughout the film may give rise to a broad distribution of lattice parameters and hence unusually and asymmetrically broadened peak in the θ–2θ scan [19] as observed in our case.

As stated earlier, the electrical properties of the pure and Si doped ZnO thin films were studied using Hall measurement in the van der Pauw four-probe configuration. The variation of electrical resistivity of the films as a function of Si concentration is shown in figure 2. The resistivity of the undoped ZnO films was found to be about $3.0 \times 10^{-2}\ \Omega$ cm. As can be seen from this figure, the resistivity first decreased rapidly and reached a minimum value of $6.2 \times 10^{-4}\ \Omega$ cm and then increased slightly with an increase in Si concentration in the films. Si being a group-IV element can act both as donor as well as acceptor. If Si occupies the Zn lattice sites or the interstitial sites it will act as a donor and if it goes to the O lattice site, it will act as an acceptor. However, the Hall

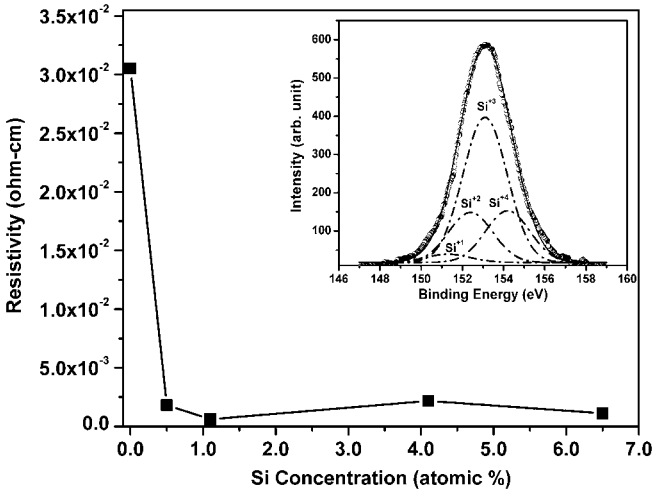

Figure 2. Variation of resistivity of the Si : ZnO thin films with Si concentration. The inset shows the XPS spectrum of the Si 2s-core level and its deconvolution into four peaks.

measurement of the films confirmed that all the films were n-type, indicating that Si was indeed acting as a donor dopant in ZnO, occupying Zn sites and donating free electrons to the ZnO lattice. The variation of n-type carrier density and mobility with Si concentration is shown in figure 3. The carrier density increased from that of the virgin films of $\sim 3.89 \times 10^{18}$ to $3.25 \times 10^{20}\ \text{cm}^{-3}$ on increasing Si concentrations up to 6.5 at% in the ZnO films. The observed carrier concentration in these films was found to be less than that of the concentration of added Si and as can be seen from figure 3, the carrier density initially increased rapidly with increasing Si concentration up to ∼1.1 at% and then steadily showing a tendency of saturation. To understand the observed behavior of Si doping in ZnO we have carried out XPS measurements on one of the representative samples (with Si concentration 4.1 at%). The

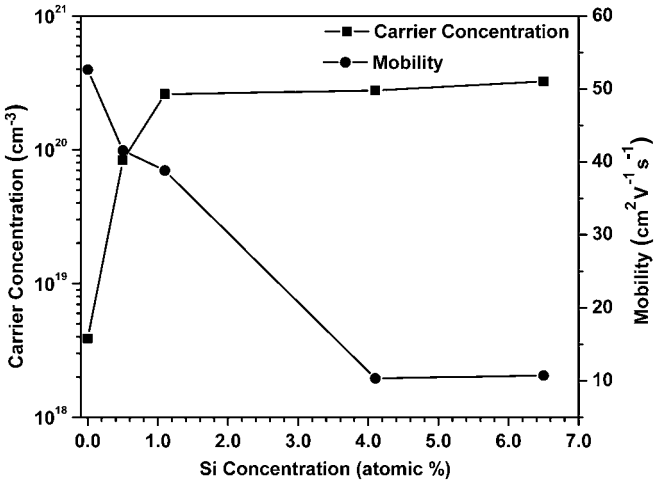

Figure 3. Variation of carrier concentration (n) and mobility (μ) in Si doped ZnO thin films with different Si concentrations.

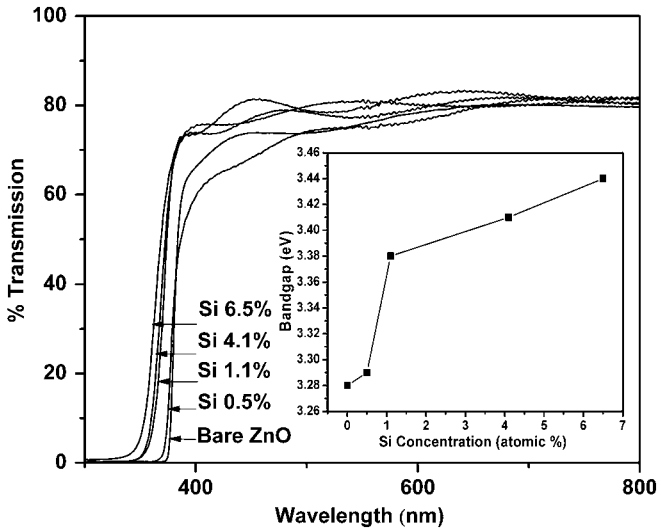

Figure 4. Transmission spectra of the Si doped ZnO thin films with different Si concentrations. Inset shows the variation of ZnO bandgap with different Si concentrations.

XPS spectrum of the Si 2s core level is shown as the inset of figure 2. This 2s peak could be deconvoluted using standard Gaussian peak fitting algorithms into four Gaussian peaks at peak energies 154.2, 153.1, 152.4 and 151.1 eV, as shown by the dashed curves in the same inset. These four peaks imply that Si actually exists in four different oxidation states in ZnO films, namely, Si^{+4}, Si^{+3}, Si^{+2}, Si^{+1} [20]. The XPS spectra did not show the presence of Si in negative oxidation states so the possibility that Si occupies the O sites and acts as an acceptor dopant in ZnO is negligibly small. The Si in the Si^{+4} state in ZnO means either the presence of SiO_2 kind of bonds or that Si goes to Zn lattice sites and donates two electrons. But the probability of the latter is energetically much lower after the donation of the first electron due to the buildup of positive charge at the Si ion. Two other peaks, namely, Si^{+2} and Si^{+1}, are possibly due to the formation of Si_2O_2 or Si_2O kind of bonds. Si in the Si^{+3} state implies that either Si is going to the Zn sites and donating one electron to the lattice or formation of Si_2O_3 kind of bonds in the ZnO lattice. Among these four possible valence states the dominating contribution is from Si^{+3} as can also be seen in the inset of figure 2. Si can donate significant free electrons in the Si^{+3} state substituting Zn in the ZnO lattice. The reason for the observed lower free electron concentration compared with the Si doping concentration in our case may be understood considering the nature of Si based oxide formation in the ZnO lattice during the growth. It is anticipated that initially when the Si doping concentration is low, the Si is predominantly substituting Zn in the ZnO lattice in the Si^{+3} state thereby donating one electron for each Si dopant and enhancing the carrier concentration rapidly. However, with increasing Si concentration in ZnO, the probability of formation of various SiO_x kinds of bonds and their segregation along grain boundaries increases. In these cases Si remains electrically inactive in the ZnO lattice and does not donate free electrons. Therefore, the carrier concentration shows a tendency to saturate. These defects do not usually contribute to the optical transmission studies and being in feeble concentration, they are also not visible in XRD patterns. This kind of variation of electron concentration with increasing doping concentration has also been reported in Ga doped ZnO films where at higher Ga concentrations Ga–O bond formation occurs at the grain boundaries [21], which does not contribute further to carrier concentration. Figure 3 also shows the variation of mobility with Si concentration. The mobility of the undoped ZnO films, which was $\sim$52 cm^2 V^{-1} s,$^{-1}$ was found to decrease with increasing Si concentration and reached a minimum value of $\sim$10 cm^2 V^{-1} s^{-1} for higher Si concentrations. The decrease in mobility is apparently due to the increase in the carrier density and the resulting electron–electron scattering, some deterioration in the crystalline quality and formation of SiO_x at the grain boundaries. This also explains the observation, stated earlier, of a slight increase in the resistivity beyond Si concentration of about 1.1 at% as shown in figure 2.

Transmission spectra of the films were recorded using a UV–visible spectrophotometer in the wavelength range from 250 to 800 nm, which are shown in figure 4. All the films were found to be highly transparent with an average transmission of $\sim$80% in the visible spectral range. Using these transmission spectra the bandgaps of these films were calculated from the α^2 versus $h\nu$ plot by extrapolating the linear portion of the curve to $h\nu = 0$. Variation of the ZnO bandgap with increasing Si doping concentration is shown in the inset of figure 4. It is clear that the bandgaps of the films monotonically increased from about 3.28 to 3.44 eV as the Si concentration was increased from 0 to 6.5 at%.

To explain the observed increase in the bandgaps of ZnO thin films with increasing Si concentration we propose that this is due to the competing effects of the BM shift [22, 23] and the bandgap narrowing, reported earlier by Jain and Roulston [24]. The BM shift in the Si doped ZnO films is inevitable because of the observed increase in the electron density as shown in figure 3. To calculate the BM shift (ΔE_{BM}) and the resulting bandgap (E_{BM}) we used the standard expressions

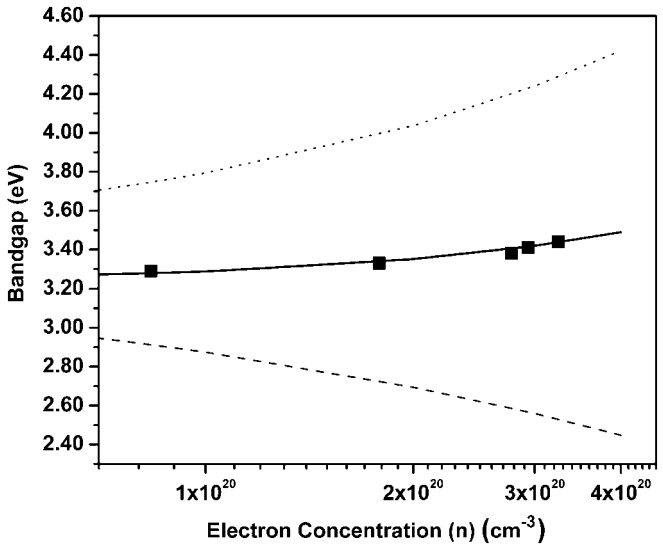

Figure 5. Variation of ZnO bandgap with carrier concentration. Filled squares are the experimental data points measured from the transmission spectra. The dotted curve is the theoretical bandgap calculated considering only the BM shift, whereas the dashed curve is the bandgap calculated using only bandgap narrowing effect. The continuous line curve in the figure is the bandgap calculated considering collective effect of both.

given in [22, 23], which are as follows:

$$\Delta E_{\mathrm{BM}} = \frac{h^2}{8\pi^2}(3\pi^2 n)^{2/3}\left(\frac{1}{m_{\mathrm{e}}^*} + \frac{1}{m_{\mathrm{h}}^*}\right), \tag{1}$$

$$E_{\mathrm{BM}} = E_0 + \Delta E_{\mathrm{BM}}. \tag{2}$$

In equation (1), while h and π are the usual constants, n is the electron density measured at different Si concentrations as shown in figure 3, the effective mass of electrons (m_{e}^*) was taken to be $0.28m_{\mathrm{e}}$ and that of the holes (m_{h}^*), $0.59m_{\mathrm{e}}$ in terms of the free electron mass (m_{e}) from [1, 11, 25]. In equation (2), E_0 is the bandgap of undoped stoichiometric ZnO representing energy separation between the ZnO conduction and the valence band without including excitons and taken to be ~3.38 eV at room temperature [1–3]. Variation in the bandgap of ZnO films with increasing carrier concentration, i.e. at increasing Si concentration, calculated from the above formula of the BM shift is shown in figure 5 by the dotted curve. The experimental values of the bandgap are shown by the filled squares in the same figure. As can be seen from the dotted curve and the experimental points, the bandgap obtained from the BM shift alone is higher and it increases faster than that observed experimentally. Thus, the BM shift alone cannot explain the observed bandgap variation with the carrier concentration

In view of the above finding it is imperative to look for other possibilities, which result in the decrease in the bandgap with increasing carrier concentration to compensate for the values calculated from the BM shift alone. We applied the concept of bandgap narrowing developed for heavily doped semiconductors [1, 26–28], which was later treated extensively by Jain and Roulston to deduce an expression applicable to any heavily doped semiconductor [24]. The bandgap narrowing is known to result from many body interactions between the carriers and interactions between carriers and impurities [1, 24, 26–28]. In n-type semiconductors, beyond a certain doping concentration, semiconductor to metal transition occurs, which is marked by the merging of the conduction band and the donor band [11, 29]. The corresponding carrier concentration is known as Mott critical density. For ZnO, the critical density has been experimentally found to vary between $\sim 5.4 \times 10^{19}$ and $8.4 \times 10^{19}\,\mathrm{cm}^{-3}$ [11, 29]. At or above this critical density, which indeed is the scenario in this case, many body interactions become effective.

To calculate the bandgap of Si doped ZnO as a function of carrier concentration due to bandgap narrowing we used the formulation reported by Jain and Roulston [24]. The same formulation has also been used earlier by Lu *et al* for Al doped ZnO thin films [11]. According to this formalism, there are four effects causing the bandgap narrowing: (i) shift of the conduction band edge due to exchange interaction amongst the electrons (ΔE_{ex}), (ii) shift of the valence band edge due to electron–hole interaction (ΔE_{eh}), (iii) shift of conduction band edge due to electron–impurity interaction (ΔE_{ei}) and (iv) shift of the valence band edge due to hole–impurity interaction (ΔE_{hi}). All the shifts are into the gap and the total energy shift (ΔE_{BGN}), i.e. bandgap narrowing is given by

$$\Delta E_{\mathrm{BGN}} = \Delta E_{\mathrm{ex}} + \Delta E_{\mathrm{eh}} + \Delta E_{\mathrm{ei}} + \Delta E_{\mathrm{hi}}. \tag{3}$$

As calculated by Jain and Roulston [24] this expression simplifies to the following formula under the assumption that electron concentration is equal to the donor concentration:

$$\Delta E_{\mathrm{BGN}} = 1.83\frac{\Lambda}{N_{\mathrm{b}}^{1/3}}\frac{R}{r_{\mathrm{s}}} + \frac{0.95R}{r_{\mathrm{s}}^{3/4}} + \left[1 + \frac{m_{\mathrm{min}}}{m_{\mathrm{maj}}}\right]\frac{1.57R}{N_{\mathrm{b}}r_{\mathrm{s}}^{3/2}}. \tag{4}$$

Here Λ is the correction factor due to anisotropy in the conduction band. It is usually in the range from 0.75 to 1 [28, 30, 31]. In our calculations the effect of band anisotropy was ignored by assuming $\Lambda = 1$ in accordance with the available literatures [11, 30, 31]. N_{b} is the number of equivalent valleys in the conduction band for n-type semiconductors and its value can be taken to be 1 [11, 30, 31]. R is given by

$$R = \frac{13.6m_{\mathrm{r}}}{\varepsilon_{\mathrm{r}}^2}\,\mathrm{eV}, \tag{5}$$

where m_{r} is the ratio of the effective mass of electrons in the conduction band and the free electron mass. The value of m_{r} has been taken to be 0.28 [1, 11, 25]. ε_{r} is the dielectric constant of Si doped ZnO. Since its value is unavailable, we have assumed it to be equal to the dielectric constant of pure ZnO films. This assumption is valid because the doping concentration is rather small. The value of ε_{r} for pure ZnO is 8.65 [11]. r_{s} is given by

$$r_{\mathrm{s}} = \frac{r_{\mathrm{a}}}{a}, \tag{6}$$

where r_{a} is half the average distance between the donor atoms and a is the effective Bohr radius of the donors. The values

of r_a and a are calculated using the formulation from [24], which are

$$r_a = \left(\frac{3}{4\pi N}\right)^{1/3}, \tag{7}$$

$$a = \frac{0.53\varepsilon_r}{m_r} \times 10^{-8}\,\text{cm}. \tag{8}$$

Here N is the impurity (in this case, donor) concentration. As discussed earlier, each Si donor gives one electron to the ZnO lattice. Moreover, other donors such as Zn interstitials (Zn_i) and oxygen vacancies (V_O) are also primarily singly ionized so that N is equal to the electron concentration, which in our case was measured as shown in figure 3. m_{maj} and m_{min} are the majority carrier (electrons) and minority carrier (holes) effective masses, respectively. We have used equation (4) for calculating the bandgap narrowing under the aforesaid assumptions. The bandgap of Si doped ZnO thin films considering only bandgap narrowing is given by

$$E_{BGN} = E_0 - \Delta E_{BGN}. \tag{9}$$

The variation of E_{BGN} with carrier concentration is shown by the dashed curve in figure 5. The total bandgap (E_{tot}) considering both the BM shift as well as bandgap narrowing is given by

$$E_{tot} = E_0 + \Delta E_{BM} - \Delta E_{BGN}. \tag{10}$$

The solid line curve in figure 5 shows the variation of the theoretical bandgap as calculated from (10) with carrier concentration. As mentioned earlier, the bandgaps of the films measured from the transmission spectra are shown by filled squares. Now it can be seen that the experimentally observed bandgap variation of Si doped ZnO thin films matches quite well those calculated from the theory. This in turn also substantiates the fact that each Si donor contributes one electron to the ZnO lattice.

Room temperature PL was studied for all the films, essentially to see the bandgap and other luminescence characteristics. The PL spectra of these films are shown in figure 6. As can be seen, the intensity of the PL peak was found to decrease with increasing Si concentration in the films. This could be due to deterioration in the crystalline quality of the films with increasing Si concentration. This is in line with the observation made by HRXRD studies which indicated deterioration in the crystalline quality of ZnO with increasing Si doping. The FWHM of the PL peak was found to increase from ∼144 to 198 meV. This increase in the FWHM of the PL peak can be attributed to the increasing deterioration of the crystalline quality and the resulting potential fluctuation due to random distribution of the impurity ions [32, 33], i.e. Si in ZnO. All the films also showed Stokes shift of the bandgap measured from PL as compared with the absorption data. The Stokes shift was found to increase from ∼27 to 187 meV with increasing Si doping. The reason for this Stokes shift in Si doped ZnO is not very well understood; however, in the literature for heavily doped n-type ZnO, it has been attributed to the different natures of absorptive and emissive optical transitions. In n-type ZnO the absorptive optical transition is from the valence band to the Fermi level whereas the emissive transition is from the donor band to the valence band. Because of this difference the luminescence peak is red shifted, i.e. Stokes shifted as compared with the absorption edge [32]. The values of the Stokes shifts in our samples compare quite well with those found in Ga doped ZnO films (22–396 meV) as reported by Makino *et al* [32] for the corresponding electron concentrations up to ∼3×10^{20} cm^{-3}.

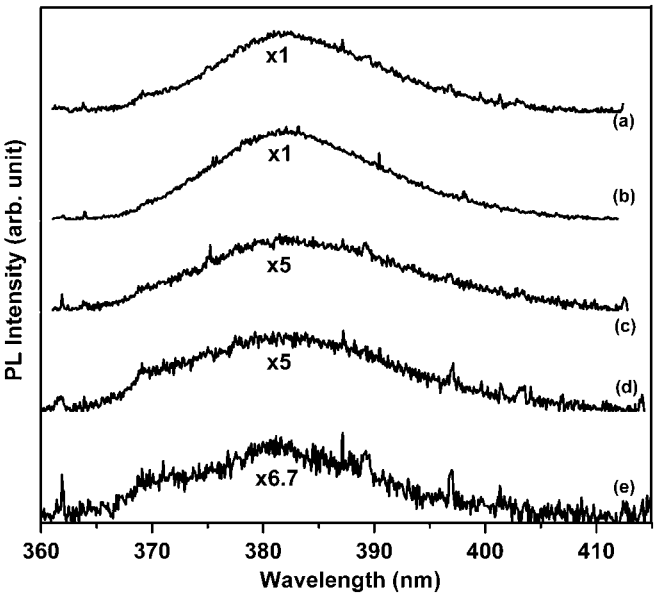

Figure 6. Room temperature PL spectra of (a) ZnO and Si doped ZnO thin films with different Si concentrations of (b) 0.5%, (c) 1.1%, (d) 4.1% and (e) 6.5%.

4. Conclusions

In conclusion, highly transparent and c-axis oriented Si doped ZnO films were grown by sequential pulsed laser deposition on the sapphire substrates. The resistivity of these films was found to decrease rapidly to a minimum and then increase slightly with increasing Si doping. This decrease in resistivity is due to enhancement in the carrier density. Blue shift in the ZnO bandgap due to Si doping was explained collectively considering the BM shift and the bandgap narrowing due to many body effects arising out of enhanced carrier and impurity concentration. On the basis of XPES and electrical measurements, it was concluded that Si atoms predominantly go to the Zn lattice sites in the Si^{+3} state and therefore Si acts as an effective donor in ZnO. Further, room temperature near band edge PL was observed in all the films which indicate reasonably good crystalline quality. Such Si doped ZnO thin films can be used as TCEs in display panels, solar cells, transparent memory devices and other emerging transparent electronic devices such as resistive non-volatile memories.

Acknowledgments

The authors wish to thank Dr B N Singh, Dr Tapas Ganguli and Mr R Kumar and Dr S M Oak of our centre for their help

in experiments and HRXRD measurements. Thanks are also due to Ms P Tiwari and Dr S K Deb of our centre for their help in EDX measurements and Dr D M Phase of CSR, Indore, for his help in the XPES measurement.

References

[1] Sernelius B E, Berggren K-F, Zin Z-C, Hamberg I and Granqvist C G 1988 *Phys. Rev.* B **37** 10244–8
[2] Myong S Y and Lim K S 2003 *Appl. Phys. Lett.* **82** 3026–8
[3] Jimenez-Gonzalez A and Suarez-Parra R 1996 *J. Cryst. Growth* **167** 649–55
[4] Zhang S B, Wei S -H and Zunger A 2001 *Phys. Rev.* B **63** 075205
[5] Look D C, Hemsky J W and Sizelove J R 1999 *Phys. Rev. Lett.* **82** 2552–5
[6] Oba F, Nishitani S R, Isotani S, Adachi H and Tanaka I 2001 *J. Appl. Phys.* **90** 824–8
[7] Jin B J, Bae S H, Lee S Y and Im S 2000 *Mater. Sci. Eng.* B **71** 301–5
[8] Van de Wale C G 2000 *Phys. Rev. Lett.* **85** 1012–5
[9] Bhosle V, Tiwari A, and Narayan J 2006 *J. Appl. Phys.* **100** 033713
[10] Lee B-T, Kim T-H, and Jeong S-H 2006 *J. Phys. D: Appl. Phys.* **39** 957–61
[11] Lu J G *et al* 2007 *J Appl. Phys.* **101** 083705
[12] Bhosle V, Tiwari A and Narayan 2006 *Appl. Phys. Lett.* **88** 032106
[13] Park S M, Ikegami T and Ebihara K 2006 *Thin Solid Films* **513** 90–4
[14] Park S M, Ikegami T and Ebihara K and Shin P K 2006 *Appl. Surf. Sci.* **253** 1522–7
[15] Minami T, Sato H, Nanto H, Takata S 1986 *Japan. J. Appl. Phys.* **25** L776–9
[16] Yan M, Lane M, Kannewurf C R and Chang R P H 2001 *Appl. Phys. Lett.* **78** 2342–4
[17] Misra P, Sahoo P K, Tripathi P, Kulkarni V N, Nandedkar R V and Kukreja L M 2004 *Appl. Phys.* A **78** 37–40
[18] Škriniarová J, Kovác J, Haško D, Vincze A, Jakabovic J, Jánoš L, Veselý M, Novotný I, Bruncko 2008 *J. Phys.: Conf. Ser.* **100** 042031
[19] Singh S, Kumar R, Ganguli T, Srinivasa R S and Major S 2008 *J. Cryst. Growth* **310** 4640–6
[20] Bekkay T, Sacher E and Yelon A 1989 *Surf. Sci.* **217** L377
[21] Ma Q-B, Ye Z-Z, He H-P, Hu S-H, Wang J-R, Zhu L-P, Zhang Y-Z and Zhao B-H 2007 *J. Cryst. Growth* **304** 64–8
[22] Burstein E 1954 *Phys. Rev.* **93** 632–3
[23] Moss T S 1954 *Proc. Phys. Soc.* B **67** 775
[24] Jain S C and Roulston D J 1991 *Solid-State Electron.* **34** 453–65
[25] Meyer B K *et al* 2004 *Phys. Status Solidi* b **241** 231–60
[26] Mahan G D 1980 *J. Appl. Phys.* **51** 2634
[27] Serre J and Ghazali A 1983 *Phys. Rev.* B **28** 4704–15
[28] Berggren K -F and Sernelius B E 1981 *Phys. Rev.* B **24** 1971–86
[29] Mott N F 1961 *Phil. Mag.* **6** 287
[30] Jain S C, Mcgregor J M and Roulston D J 1990 *J. Appl. Phys.* **68** 3747–9
[31] Moysés Araújo C *et al* 2002 *Microelectron. J.* **33** 365
[32] Makino T, Segawa Y, Yoshida S, Tsukazaki A, Ohtomo A and Kawasaki M 2004 *Appl. Phys. Lett.* **85** 759–61
[33] Schubert E F, Goepfert I D, Grieshaber W and Redwing J M 1997 *Appl. Phys. Lett.* **71** 921–3